Quasiparticle and thermodynamic mass in the heavy-fermion system $CeB_6$



1993 J. Phys.: Condens. Matter 5 7435

(http://iopscience.iop.org/0953-8984/5/40/018)

J. Phys.: Condens. Matter 5 (1993) 7435–7450. Printed in the UK

# Quasiparticle and thermodynamic mass in the heavy-fermion system $CeB_6$

N Harrison, P Meeson, P-A Probst and M Springford
*H H Wills Physics Laboratory, University of Bristol, Tyndall Avenue, Bristol BS8 1TL, UK*

Received 1 July 1993

**Abstract.** The de Haas–van Alphen effect has been investigated in the heavy-fermion compound $CeB_6$ in magnetic fields extending to 53 T. Absolute amplitude measurements reveal that the major sheets of the Fermi surface are not spin polarized, and that its observed volume is $1.15 \pm 0.1$ electrons per formula unit. Analysis of the field dependence of the quasiparticle effective mass based on the periodic Anderson model yields, for the ratio of the characteristic temperature to the $g$ factor, $T^*/g = 4.0 \pm 0.8$ K, while over the field interval 31–43 T, for which the mass changes by a factor of two, the mean free path of the quasiparticles remains constant at $56 \pm 1$ nm. We compare the density of states derived from the measured quasiparticle masses with that deduced from specific-heat experiments for magnetic fields below $\sim 30$ T, and find them to be in agreement. We conclude that the low-temperature thermodynamics of $CeB_6$ may be understood simply in terms of the low-energy excitations of a heavy charged Fermi liquid. We note that these experiments do not support the idea of Kagan *et al* that a significant contribution to the low-temperature thermodynamics of Ce-based heavy-fermion systems arises from the presence in them of a neutral Fermi liquid.

## 1. Introduction

Certain ordered metallic compounds, containing either rare-earth or actinide elements, exhibit properties at low temperatures that are consistent with the presence in them of an abnormally heavy Fermi liquid. Characteristically this is reflected by a large density of states at the Fermi energy, which may, for example, be $\sim 1000$ times larger than that expected for a normal metal or, equivalently, by comparably large values of the quasiparticle masses. While some understanding of the origin of these strong enhancements is obtained using the periodic Anderson model, a theoretical approach capable of yielding material-specific parameters is an important and challenging problem. The results of Landau quantum-oscillation experiments, such as the de Haas–van Alphen (DHVA) effect, have added richly to this debate by providing detailed information on the Fermi surface, and on the dynamical properties of the quasiparticles, in a number of heavy-fermion systems [1–3]. By means of these experiments one can also address such fundamental issues as the nature of the Fermi liquid state and the validity of Luttinger's theorem in the presence of such strong renormalization. While it is difficult to discern a universal behaviour amongst these metals, $CeB_6$ displays many of the characteristics regarded as typical of heavy fermions.

The rare-earth hexaborides ($ReB_6$: Re = La, Ce, Pr, Nd and Sm) have provided an interesting laboratory for both experiment and theory during recent years. Crystallizing in the cubic $CaB_6$ structure, which may be viewed as the CsCl structure in which the B octahedra replace Cl atoms, they display a variety of ground states. With an empty 4f shell, $LaB_6$ is a paramagnetic metal, whereas both $PrB_6$ and $NdB_6$ are localized 4f

0953-8984/93/407435+16$07.50  

systems with magnetic order. $PrB_6$ orders magnetically with a double-$k$ structure which is at first incommensurate ($T_N = 6.9$ K) and then commensurate ($T_C = 3.9$ K), while $NdB_6$ is a simple antiferromagnet ($T_N = 8.5$ K). $SmB_6$ is a 'semiconducting' mixed-valence compound, having a gap in the narrow f band at the Fermi energy. $CeB_6$, however, is a dense Kondo compound in which the Kondo effect competes with exchange interactions to produce the unusual phase diagram shown in figure 1 [4]. Two ordering transitions occur: a quadrupolar ordering temperature $T_Q = 3.2$ K and a Néel temperature $T_N = 2.3$ K, both of which are strongly dependent on the applied field. In phase I, the electrical resistivity exhibits a typical ($-\ln T$) Kondo behaviour with $T_K \sim 2$ K. Phase II has been identified by neutron scattering [4,5] as an ordered antiferroquadrupolar phase with wavevector $[\frac{1}{2}, \frac{1}{2}, \frac{1}{2}]$, corresponding to a doubling of the unit cell along the three cubic directions, while in phase III, $CeB_6$ is antiferromagnetically ordered with a double-$k$ commensurate structure [6]. At low temperatures in the magnetically ordered phase the large electronic specific-heat coefficient, $\gamma = 250$ mJ mol$^{-1}$ K$^{-2}$ [7], is to be compared with $\gamma = 2.6$ mJ mol$^{-1}$ K$^{-2}$ [8] in the f-electron free compound $LaB_6$.

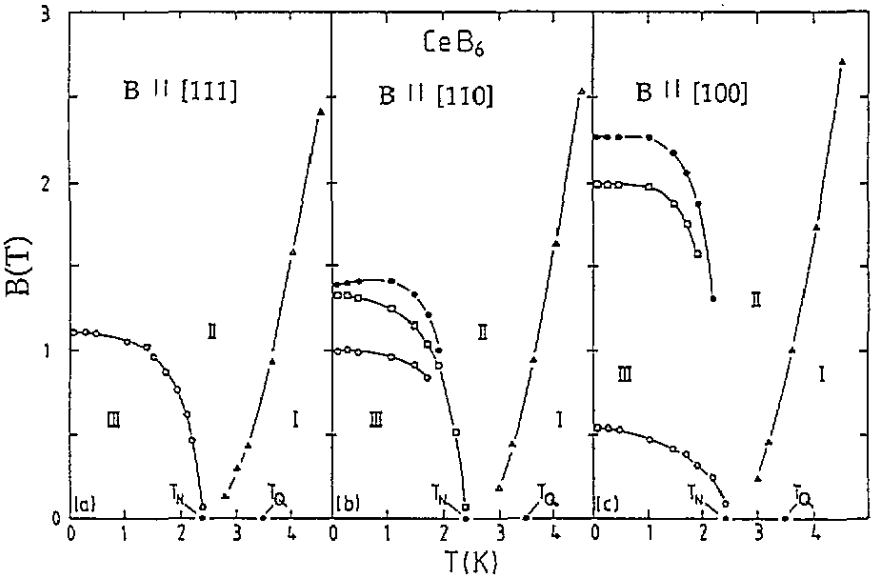


**Figure 1.** Phase diagram of $CeB_6$ in the $B$–$T$ plane for the field directed along the three principal symmetry directions [32]. I, II and III correspond to paramagnetic, antiferroquadrupolar ($T_Q = 3.2$ K) and antiferromagnetic ($T_N = 2.3$ K) phases respectively.

The first DHVA experiments in $CeB_6$ were those of van Deursen *et al* [9,10] who employed pulsed magnetic fields extending to 40 T. With hindsight it is now clear that they were able to detect signals only because, at the high fields used, the quasiparticle mass was appreciably reduced to the value of $\sim 6m_0$. The striking effect of a magnetic field in reducing the cyclotron effective mass was explicitly discovered only subsequently by Joss *et al* [11] who, for example, reported a reduction in the mass from approximately $18m_0$ at 13 T to $8m_0$ at 22 T, a variation that is qualitatively similar to that of $\gamma$ over the same field interval [7, 12].

It is instructive to compare the angle-resolved measurements of the DHVA effect in $CeB_6$ [13] with those in $PrB_6$ [14] and $LaB_6$ [15, 16]. The main Fermi surface feature in each case

consists of a set of three equivalent nearly spherical ellipsoidal electron sheets centred at the X points of the Brillouin zone and connected by necks in the ⟨110⟩ directions. The results of band-structure calculations by Hasegawa and Yanase [17] and by Harima *et al* [18] for $LaB_6$ are depicted in figure 2. A further set of smaller electron sheets are seen to be located at the neck positions. Both the extent of the contact between the main ellipsoids and also the sizes of the smaller ellipsoids vary considerably between the different compounds. In $PrB_6$ the situation is complicated by the presence of additional zone boundaries introduced by the antiferromagnetic order although, in the fields used to investigate the DHVA effect, magnetic breakdown appears to be sufficient so as to largely reveal the 'underlying' paramagnetic Fermi surface, with few signatures of the AFM Fermi surface.

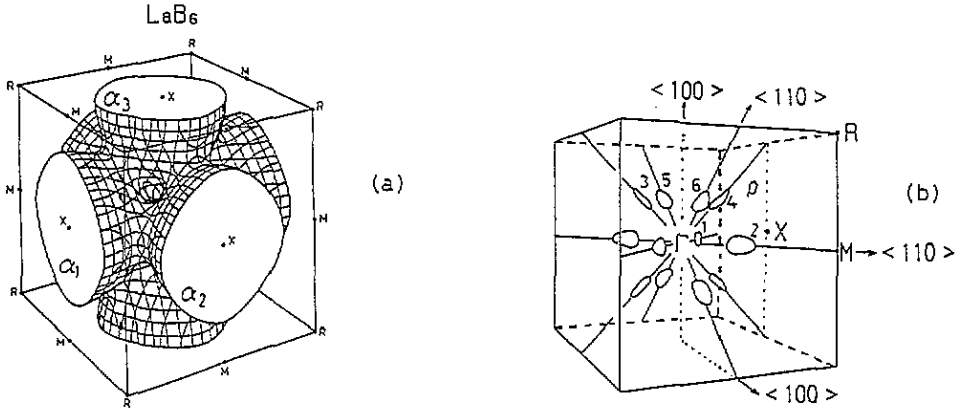


**Figure 2.** Fermi surface of $LaB_6$ showing in (*a*) the main multiply connected electron ellipsoidal surfaces from Hasegawa and Yanase [17] and in (*b*) the twelve smaller ellipsoidal electron pockets according to Harima *et al* [18].

Given a knowledge of the Fermi surface in $CeB_6$, together with the variation of the quasiparticle velocity $v^*$ over it, one may calculate the quasiparticle density of states $N_{QP}(E_F)$, for comparison with that ($N_{SH}(E_F)$) derived from the electronic specific heat, defined as follows:

$$N_{QP}(E_F) = \frac{1}{4\pi^3\hbar}\int_s \frac{dS}{|v^*|} \tag{1}$$

$$N_{SH}(E_F) = 3\gamma/\pi^2 k_B^2. \tag{2}$$

As a detailed knowledge of the Fermi surface $S$ and the quasiparticle velocity $v^*$ was incomplete, previous calculations [1] have been based on a model in which the Fermi surface was approximated by three spheres centred at the X points (the radial anisotropy of the Fermi surface in $CeB_6$ is 16% [13]) and the effects of the neck regions and smaller ellipsoids were ignored. The result is to replace equation (1) by

$$N_{QP}(E_F) \cong \frac{1}{4\pi^3\hbar}\sum_i \frac{\bar{S}_i}{\bar{v}_i} = \frac{m_e}{\pi^2\hbar^2}\left(\frac{2e}{\hbar}\right)^{1/2}\sum_i F_i^{1/2}\frac{m_i^*}{m_e} \tag{3}$$

in which $\bar{v}_i$ and $\bar{S}_i$ are averaged values, for which we have written $\bar{v}_i = \hbar k_i/m_i^*$ and $\bar{S}_i = 4\pi k_i^2 = 8\pi e F_i/\hbar$. Evaluating equations (2) and (3) for the three-sphere model

($\sum_i = 3$) using the measured values at 12.7 T of $\gamma = 120$ mJ mol$^{-1}$ K$^{-2}$ [12] and $m^*/m = 14.0$ [13], and taking for $F$ the value at ⟨100⟩ of $F = 8670$ T, yields for the densities of states

$$N_{QP}(E_F) = 1.8 \times 10^{48} \text{ states m}^{-3} \text{ J}^{-1} \qquad N_{SH}(E_F) = 4.5 \times 10^{48} \text{ states m}^{-3} \text{ J}^{-1}.$$

Including the 12 smaller electron sheets in the same approximate way, using the measured parameters given by Onuki *et al* [13], only increases $N_{QP}(E_F)$ by $\sim 0.2 \times 10^{48}$ state m$^{-3}$ J$^{-1}$, so that there appears to be a discrepancy between the values of the densities of states determined in the two experiments. We are therefore led to ask whether our knowledge of the Fermi surface is incomplete, or whether the enhanced specific heat may have a contribution other than from the quasiparticles.

On the basis of a comparison with the experiments in $PrB_6$, one may argue [13] that, in high magnetic fields, the up- and down-spin Fermi surfaces will be different, and that only the up-spin sheet with lower mass may have been detected to date in the DHVA experiments in $CeB_6$. This explanation receives support from the work of Langford *et al* [19], who calculated the electronic properties of the rare-earth hexaborides within the framework of density-functional theory. It follows from this explanation that such a heavy sheet, if it exists, will be revealed by performing experiments under the appropriate conditions of low temperature and high magnetic field. We note the recent measurements of the DHVA effect in $CeB_6$ in magnetic fields extending to 52 T by Haanappel *et al* [20]; a striking feature of their work being a sudden disappearance of the DHVA signals for temperatures above 2.3 K.

Recently, Kagan *et al* [21] have presented arguments in favour of a picture in which *neutral* Fermi excitations of spin origin contribute significantly to the thermodynamics of heavy-fermion systems with nearly integer valence, such as the Ce-based systems. Their picture results in an unusual two-component Fermi liquid in which the heavy neutral fermions contribute to the specific heat at low temperatures by an amount that is linear in temperature and also couple to the conduction electrons within an energy interval $T_K$ leading, at $T < T_K$, to a difference between the quasiparticle and thermodynamic masses. Because only charged carriers can contribute to the diamagnetic response, it is only these that are seen in the DHVA effect, which is therefore modified by an additional temperature dependence of the amplitude arising from the inelastic interaction between the quasiparticles and the low-energy spin excitations that renormalize $\omega_c\tau$ [22, 23].

The present work was undertaken with the aim of clarifying these uncertainties, particularly with regard to the apparent discrepancy between the *quasiparticle* and *thermodynamic* masses.

## 2. Experimental details

Experiments were performed using a nominal 60 T pulsed-field DHVA effect spectrometer, the details of which have been described elsewhere [24]. The sample was immersed in liquid $^4$He whose temperature could be varied between 4.2 K and 1.3 K as determined from its vapour pressure. During a typical pulse, the peak magnetic field was reached sinusoidally in $\sim 4$ ms, after which the magnetic field decayed exponentially, with a time constant of $\sim 10$ ms. The DHVA oscillations were detected as a voltage $V$ induced in a compensated arrangement of pick-up coils wound concentrically around the sample and coupled to it with coupling constant $\eta$, such that

$$V = \eta\Omega(\partial B/\partial t)\partial\tilde{M}/\partial B \tag{4}$$

in which $\Omega$ is the volume and $\tilde{M}$ is the oscillatory magnetization. While there exists no general theory for $\tilde{M}$ in heavy-fermion systems, there is the expectation that its general form will closely resemble that derived for more normal metals by Lifshitz and Kosevich [25], modified by the strong electron correlations. Model calculations by Wasserman *et al* [26] and by Rasul [27] seem to confirm this, so that we may write

$$|\tilde{M}| = -\sum_r \left(\frac{e}{\hbar}\right)^{3/2} \frac{2Fk_BT}{(2\pi r B A'')^{1/2}} \frac{\exp(-r\pi/\omega_c\tau)\cos(\pi r g \mu_B B/2\hbar\omega_c')}{\sinh(2\pi^2 r k_B T/\hbar\omega_c^*)} \sin\left(2\pi r\frac{F}{B} + \gamma_r\right) \tag{5}$$

$A''$ being the curvature factor and $\tau$ the quasiparticle lifetime. The three different cyclotron frequencies, $\omega_c$, $\omega_c'$ and $\omega_c^*$, or equivalently effective masses, $m$, $m'$ and $m^*$, refer to values differently influenced by many-body interactions. In the exponential (scattering) term, it is normally appropriate to regard $\omega_c\tau$ as referring to the interaction between a quasiparticle and static defects or impurities and being unrenormalized by other interactions. In the cosine factor, which accounts for Zeeman splitting assuming that both up- and down-spin electrons contribute with equal amplitude, the renormalized value $\omega_c'$ is expected in general to include the effect of electron–electron interactions [28] and, in heavy-fermion systems, for the corresponding effective mass $m'$ to assume its zero-field-enhanced value [26]. In the sinh term, $\omega_c^*$ includes other (e.g. electron–phonon) interactions and, in heavy-fermion systems, $m^*$ is expected to vary with magnetic field [26].

The dominant contribution to $V$ originates from the rapidly changing oscillatory (sine) term in (5) to yield

$$V \cong -2\pi r\eta\Omega(F/B^2)\tilde{M}\,\partial B/\partial t = a(B,T)\sin(2\pi r F/B + \gamma_r) \tag{6}$$

$$a(B,T) = \sum_r c(B)\frac{T}{\sinh(2\pi^2 r k_B T/\hbar\omega_c^*)} \tag{7}$$

$$c(B) = 4\pi\eta\Omega(F^2/B^{5/2})(\partial B/\partial t)(e/\hbar)^{3/2}[r^{1/2}k_B/(2\pi A'')^{1/2}] \times \exp(-r\pi/\omega_c\tau)\cos(\pi r g\mu_B B/2\hbar\omega_c'). \tag{8}$$

The rate of change of magnetic field was measured simultaneously with $V$ using a separate pick-up coil, and the magnetic field was subsequently found by numerical integration of the recorded induced voltage. As it was only possible to directly compensate the DHVA detection coil of $\sim$ 200 turns to $\pm 0.5\%$ against changes of the main magnetic field, a component from the field measuring channel was added to the signal channel to achieve a high degree ($\sim 0.01\%$) of compensation. The two voltages were amplified and recorded synchronously at 2 $\mu$s intervals with a resolution of 12 bits, using a National Instruments NB-A2000 input board and a Macintosh IIfx computer.

A single crystal of $CeB_6$, of mass $3.29 \pm 0.06$ mg and volume $\sim 0.7$ mm$^3$, which had been used previously by us for DHVA effect studies at lower magnetic fields [13], was oriented with the field directed along [001]. Measurements of the DHVA amplitudes for different rates of change of magnetic field revealed a significant rise in temperature of the sample due to eddy-current heating by up to $\sim 0.5$ K, depending on the experimental conditions. Several slots were therefore cut into the sample, parallel to the field direction, by spark erosion which reduced the sizes of the eddy-current orbits and improved the thermal coupling of the sample to the liquid-$^4$He bath by increasing the surface area of the sample. The net effect was to reduce the temperature rise by two orders of magnitude, such that the uncertainty in our knowledge of the sample temperature in superfluid He was less than 10 mK under the most unfavourable conditions.

## 3. Results

Experiments were performed in $CeB_6$ in magnetic fields up to $\sim 53$ T and in liquid $^4$He at temperatures down to 1.3 K. An example of the signal obtained in a 45 T pulse is shown in figure 3(*a*), where oscillations are seen in both rising and falling fields. The amplitude spectrum of the quantum oscillations computed by the method of maximum entropy is shown in figure 3(*b*), and is seen to reveal the presence of five DHVA frequencies. The signal is dominated by the frequency $F = 8670$ T and its harmonic at 17 340 T. Two further features at $\sim 11\,000$ T and $\sim 13\,400$ T are found to be present at the highest fields. Low-frequency signals, corresponding here to the smaller electron ellipsoids, are weak in such a pulsed-field experiment, consistent with the fact that the sensitivity is seen, from equation (8), to vary as $F^2$. The frequency of $\sim 11\,000$ T may be the result of magnetic breakdown taking place between the larger and smaller electron surfaces in the regions of the necks, thereby allowing an extremal orbit $\alpha'$ to be seen, approximating to the shaded area of one of the larger ellipsoids in figure 4. The frequency $F \simeq 13\,400$ T, may correspond to a non-central extremal orbit, the effective mass in table 1 being consistent with this. The spectral feature in figure 3(*b*) at $\sim 60$ kT is the angle-averaged Cu 'belly' frequency, and originates from the coarsely polycrystalline nature of the Cu comprising the pick-up coils. This is present even in the absence of a sample and provides a useful calibration.

**Table 1.** Cyclotron masses in $CeB_6$ measured in magnetic fields of 40.1 T and 44.4 T directed along [001], for the DHVA frequencies $F = 11\,000$ T and $F = 17\,340$ T.

| Magnetic field (T) | $F = 11\,000$ T | $F = 17\,340$ T |
|---|---|---|
| 44.4 | $1.4 \pm 0.4 m_e$ | $4.3 \pm 1.2 m_e$ |
| 40.1 | $3.1 \pm 1.6 m_e$ | $4.8 \pm 1.0 m_e$ |

A striking observation in all of these experiments was the abrupt disappearance of the DHVA effect at a temperature of $2.17 \pm 0.01$ K, i.e. at the lambda transition for superfluid $^4$He. We attribute this to the poor thermal coupling to the sample when it is immersed in liquid $^4$He in the *normal* fluid state. We believe therefore that the similar observation by Haanappel *et al* [20] is also attributable to this affect and not, as they conjectured, to some kind of phase transition occurring at 2.3 K.

## 4. The variation of the effective mass

To find the cyclotron mass $m^*(B)$ as a function of magnetic field, for the $\alpha$ orbit, the measured amplitude $a(B, T)$ of the DHVA signal, in equation (6) was fitted to equation (7) over the temperature range 1.3–2.17 K, with $c(B)$ and $\omega_c^*$ as adjustable parameters. This procedure was followed throughout the field range 36–47 T and the resulting values for $m^*(B)$, when combined with those found previously at lower fields, are shown in figure 5.

A theory for the DHVA effect in heavy-fermion systems, based on the Anderson lattice model [26], links the quenching of the heavy mass in high magnetic fields with Zeeman splitting of the many-body band at the Fermi energy, which arises from the combined effects of hybridization and Coulomb interaction between the conduction and f electrons. In the simplest case of $J = \frac{1}{2}$, it is the effective mass of the up-spin channel that is quenched by the magnetic field initially. Following Wasserman *et al* [26],

$$m^*(B)/m_b = 1 + \xi_1/(1 + \xi_2 B)^2 \tag{9}$$

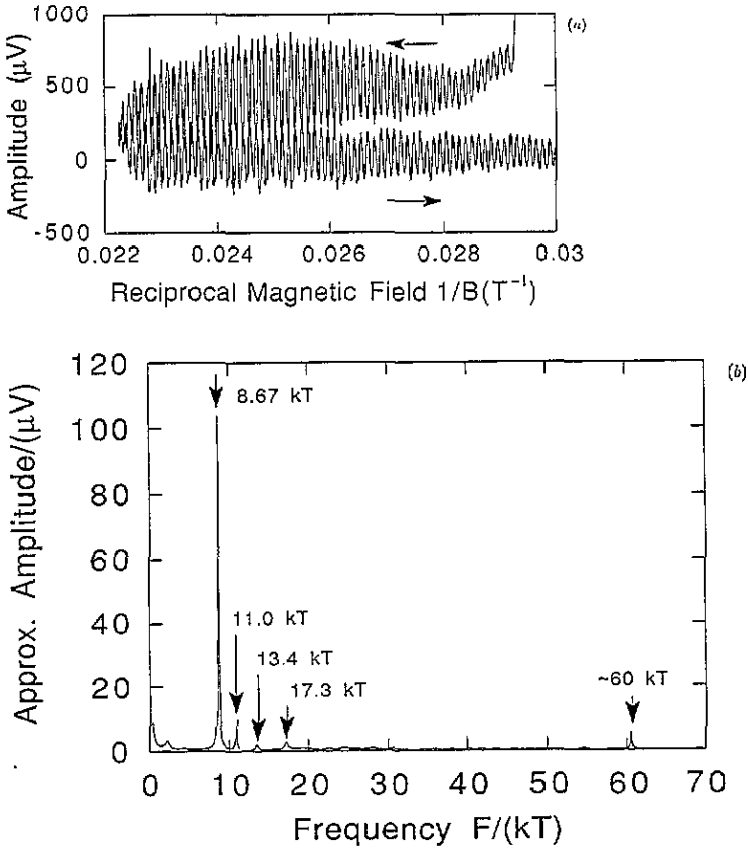


**Figure 3.** (*a*) DHVA effect signal in $CeB_6$ at 1.3 K recorded using a pulsed magnetic field. The amplitude is greater on the rising side of the pulse because of the greater value of $dB/dt$. (*b*) Amplitude spectrum of the DHVA signal in (*a*) calculated by the method of maximum entropy. The signal at ~ 60 kT provides a useful calibration as it is the angle-averaged 'belly' frequency of Cu and originates from the Cu pick-up coil itself.

in which $\xi_1$ and $\xi_2$ are given by

$$\xi_1 = 2Dn_f/Nk_BT^* \qquad \xi_2 = (J/k_BT^*)g\mu_B \tag{10}$$

where $m_b$ is the bare band mass, $D$ is the bare bandwidth, $n_f$ is the mean occupancy of the 4f levels, $g$ is the electron $g$ factor, $\mu_B$ is the free-electron Bohr magneton, $T^*$ is the characteristic temperature and $N = 2J + 1$. The best fit to the experimental data, which is indicated by the full curve in figure 5, yields for $\xi_1$ and $\xi_2$ the values $\xi_1 = 260 \pm 80$ and $\xi_2 = 0.16 \pm 0.03\ T^{-1}$.

The free $Ce^{3+}$ ion has a single 4f electron and $J = \frac{5}{2}$. In a cubic crystal field, the degeneracy of this multiplet is known to be resolved into a doublet, $\Gamma_7$, and a quartet, $\Gamma_8$. A careful study of the susceptibility [29] indicates that the $\Gamma_8$ multiplet forms the ground state of the system, implying that $J = \frac{3}{2}$. However, the DHVA effect is here observed in the antiferroquadrupolar phase II. In this regime, studies by inelastic neutron scattering [4] show the $\Gamma_8$ multiplet to be split into two doublets, so $J = \frac{1}{2}$. Using this value and the above relation for $\xi_2$, we find for the ratio $T^*/g = 4.0 \pm 0.8$ K, where $g$ is unknown but expected to be of the order of one or two. This compares favourably with estimates based

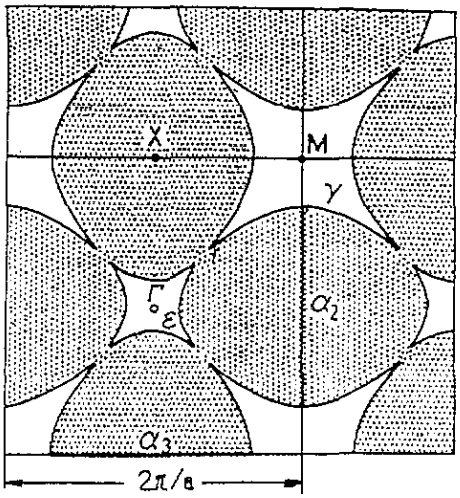


**Figure 4.** Schematic diagram of the Fermi surface of $CeB_6$ in the X–M plane of the simple cubic Brillouin zone, showing the $\alpha$, $\varepsilon$ and $\gamma$ orbits. In the absence of the necks, the $\alpha'$ orbits would bound each of the shaded regions.

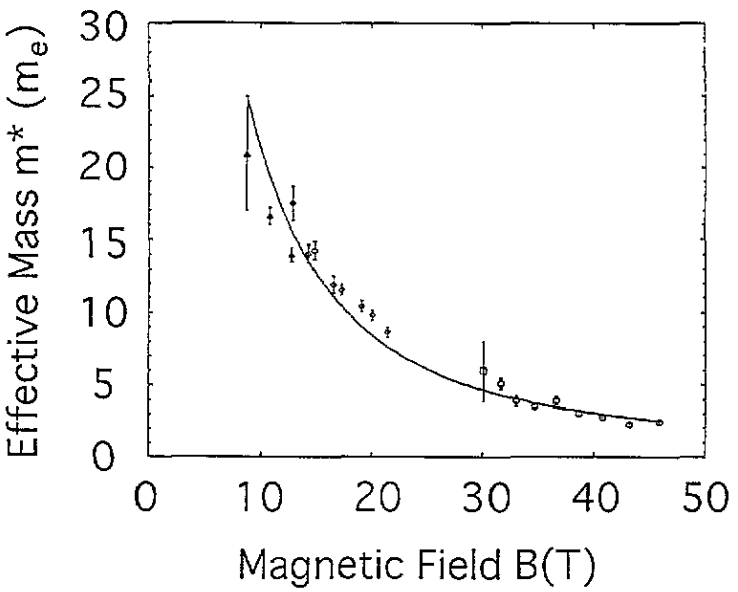


**Figure 5.** Cyclotron effective mass measured in $CeB_6$ for the magnetic field oriented along [001] for which the DHVA frequency $F = 8670$ T. Open circles are from the present work, squares from [9] and [10], diamonds from [11] and triangles from [13]. The full curve represents the best fit to the experimental data according to the theory of Wasserman *et al* [26].

on measurements of the electrical resistivity, which yield $T^* \simeq 5$–10 K or $\sim 3$ K from neutron scattering. With $N = 2J + 1 = 2$ and $n_f = 1$ (for nearly localized 4f electrons), we infer from $\xi_1$ that the width of the conduction band given by $2D/g = 0.2$–0.1 eV. On the basis of these considerations, the Anderson lattice model appears to describe the field

dependence of $m^*$ reasonably well in this material. The cyclotron masses for the other orbits were also measured, although with less accuracy, and are given in table 1. For the 17 340 T frequency, the values are consistent with it being the second harmonic of the main frequency $F = 8670$ T.

## 5. Analysis of the DHVA-effect amplitude

It follows from the above analysis that a graph (conventionally referred to as a Dingle plot) of

$$\ln A = \ln[a(B, T)B^{5/2}\sinh(2\pi^2 r k_B T/\hbar\omega_c^*)/\dot{B}T] \text{ versus } B^{-1} \tag{11}$$

has gradient

$$-r\pi m/e\tau = -r\pi l_c/l \tag{12}$$

and intercept

$$\ln[4\pi\eta\Omega F^2(e/\hbar)^{3/2}[r^{1/2}k_B/(2\pi A'')^{1/2}]\cos(\pi r g\mu_B B/\hbar\omega_c')] \tag{13}$$

where $l$ is the mean free path of a quasiparticle between collisions with static defects and impurities, and $l_c$ is the classical cyclotron length

$$l_c = (2\hbar F/eB^2)^{1/2}. \tag{14}$$

The results derived from many pulses have been averaged in figure 6 to which a linear least-squares fit yields $l = 56 \pm 1$ nm. This clearly shows that the mean free path remains constant, in spite of the fact that the effective mass $m^*$ changes with increasing magnetic field as shown in figure 5.

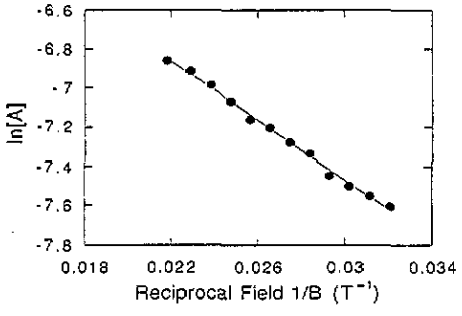


**Figure 6.** Field dependence of the DHVA effect (Dingle plot) in $CeB_6$ based on equation (11), being an average of the results derived from 10 experiments performed over the temperature range 1.3–2.1 K. The linear behaviour signifies a constant value for the quasiparticle mean free path of $56 \pm 1$ nm over the field range in which the effective mass varies by a factor of approximately two.

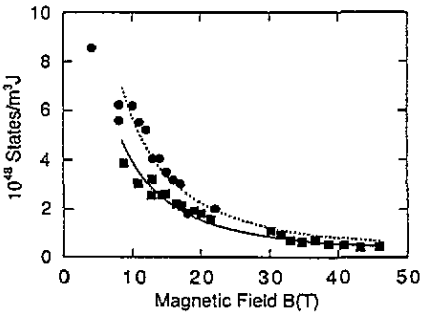


**Figure 7.** Variation of the 'quasiparticle' and 'thermodynamic' densities of states, $N_{QP}$ (squares) and $N_{SH}$ (circles) respectively, with magnetic field in $CeB_6$. $N_{SH}$ values are obtained from the specific-heat measurements of Muller *et al* [12] using equation (2). $N_{QP}$ values are derived from DHVA-effect measurements [13, 31] as described in the text. The full curve is a best fit to the DHVA-effect data according to the theory of Wasserman *et al* [26]. The broken curve refers to $N_{QP}$ with the contribution from the contact or 'neck' regions of the larger electron Fermi surface sheet included, and is in good agreement with $N_{SH}$. Parameters used in these calculations are summarized in tables 2 and 3.

For the intercept $A_0$ (with the cosine factor equal to unity) equation (13) yields

$$\ln A_0 = \ln[4.10\eta r^{1/2} F^2 \Omega/(A'')^{1/2}]. \tag{15}$$

In the present experiment, $\eta = 0.0739$ H m$^{-2}$, $\Omega = (0.54 \pm 0.01) \times 10^{-9}$ m$^3$ and $A'' = 4.67$ is the curvature factor of the cyclotron orbit estimated from the ratio between extremal areas [3]. From this we obtain $\ln[A_0] = -5.14$ in excellent agreement with the measured intercept from figure 6 of $-5.19 \pm 0.09$. The value for the intercept in the case of carriers of one spin only would be $-5.88$. From this we infer that up- and down-spin quasiparticles must contribute equally and that the cosine (Zeeman) factor has a value close to unity for all fields. These general conclusions are in agreement with the theory of Wasserman *et al* [26] for a $J = \frac{1}{2}$ system in the high field limit.

Assuming that all sheets of the Fermi surface are detected in these experiments, and that they are populated by both up- and down-spin quasiparticles, then we may infer from its volume the number of quasiparticles per formula unit. Ignoring for the moment the ⟨110⟩-directed necks, by an appropriate choice of axes the larger electron sheets may be well represented as prolate ellipsoids of revolution, as indicated schematically in figure A1(*a*).

$$(k_x^2 + k_y^2)/k_0^2 + k_z^2/r^2 k_0^2 = 1 \tag{16}$$

where $r$ is the ratio of the semi-major to semi-minor axes. The measured DHVA frequency of the ⟨001⟩ $\alpha$ orbit, $F = 8670$ T, yields for the semi-minor axis $k_0 = 5.13 \times 10^9$ m$^{-1}$. Although the $\alpha'$ orbits (shown shaded in figure 4) cannot be measured directly, their size may be estimated by extrapolation of the angle-resolved measurements of Onuki *et al* [13] to be $\sim 10\,060$ T. This is consistent with a value for the upper limit that is obtained from the condition (figure 4)

$$F_{\alpha'} < \tfrac{1}{2}(F_{BZ} - F_\varepsilon - F_\gamma) \tag{17}$$

in which $F_{BZ}$ corresponds to the ⟨100⟩ cross section of the Brillouin zone

$$F_{BZ} = (\hbar/2\pi e)(2\pi/a)^2 \tag{18}$$

and $a = 0.4141$ nm. Given $F_\varepsilon = 1300$ T and $F_\gamma = 2190$ T from Onuki *et al* [13], we obtain $F_{\alpha'} < 10300$ T. These dimensions are summarized in table 2 together with those of the 12 smaller electron ellipsoids. Allowing for the uncertainty in the volume introduced by the presence of necks, this yields $0.57 \pm 0.05$ for the occupied fraction of the Brillouin zone, equivalent to $1.15 \pm 0.1$ electrons per formula unit.

**Table 2.** Principal dimensions of the Fermi surfaces of $CeB_6$ and $LaB_6$. All sheets are approximated as prolate ellipsoids of revolution with minor and major cross sections corresponding to DHVA frequencies $F_{min}$ and $F_{max}$ and semi-minor and semi-major axes $k_0$ and $rk_0$ respectively. $V$ is the volume per ellipsoid, while the volume of the (cubic) Brillouin zone is $3.493 \times 10^{30}$ m$^{-3}$ for $CeB_6$ and $3.456 \times 10^{30}$ m$^{-3}$ for $LaB_6$.

| | $F_{min}$ (T) | $F_{max}$ (T) | $k_0$ (m$^{-1}$) | $rk_0$ (m$^{-1}$) | $r$ | $V$ (m$^{-3}$) | $m^*_{min}$ |
|---|---|---|---|---|---|---|---|
| $CeB_6$ | | | | | | | |
| Small | 70 | 400 | $4.61 \times 10^8$ | $2.63 \times 10^9$ | 5.7 | $2.34 \times 10^{27}$ | 2.0 |
| Large | 8670 | 10060 | $5.13 \times 10^9$ | $5.95 \times 10^9$ | 1.16 | $6.56 \times 10^{29}$ | 14.0 |
| $LaB_6$ | | | | | | | |
| Small | 3 | 12 | $9.5 \times 10^7$ | $3.8 \times 10^8$ | 4.0 | $1.4 \times 10^{25}$ | 0.027 |
| Large | 7890 | 10000 | $4.89 \times 10^9$ | $6.20 \times 10^9$ | 1.27 | $6.21 \times 10^{29}$ | 0.64 |

## 6. The quasiparticle and thermodynamic mass

Returning to the discrepancy between the *quasiparticle* and *thermodynamic* masses, we wish to extend our discussion in section 1 above to the more general case of Fermi sheets having the shape of ellipsoids of revolution. It has been noted by Joss *et al* [30] that effective mass measurements made over the larger electron surface at field orientations 0°, 15°, 30° and 45° from [001] in the (100) plane, and at 0°, 30° and 90° to [001] in the (110) plane are, to within the experimental accuracy, all proportional to the area of the orbit, in accordance with a generalized ellipsoidal model (cf appendix 1 of [28]). Consistent with the angle-resolved DHVA frequencies, we therefore model these sheets as prolate ellipsoids of revolution for which it may be shown (cf appendix below) that equation (3) assumes the more general form

$$N_{QP}(E_F) = (m_e/\pi^2\hbar^2)(2e/\hbar)^{1/2} F_{min}^{1/2} m^*_{min} r/m_e \tag{19}$$

in which $r$ is the ratio of semi-major to semi-minor axes, $rk_0$ and $k_0$ respectively, and $F_{min}$ is the DHVA frequency corresponding to the minimum extremal cross section, $\pi k_0^2$. Using for the parameters describing the larger electron ellipsoids the values discussed above, which are summarized in table 2, then $r = 1.16$ and therefore the density of states, $N_{QP}$, is greater by this factor than the value derived in section 1 using the spherical approximation. The same approach may be used to include the contribution to $N_{QP}$ from the 12 smaller electron ellipsoids. The most complete information on these was obtained by Matsui *et al* [31] from measurements of the acoustic DHVA effect. Although they appear to observe a weak exchange splitting of these sheets, we shall ignore this as no evidence is observed elsewhere on the Fermi surface. Consistent with the measured DHVA frequencies, we shall therefore assume that the 12 smaller electron sheets can also be approximated as prolate ellipsoids of revolution, with major and minor cross sections corresponding to $F = 400$ T

and 70 T respectively. Making the ellipsoidal approximation as before, i.e. that $F/m^*$ is constant, where $m^* = 3.5m_e$ for $F = 120$ T at $\sim 12.7$ T [13], it follows from table 2 and equation (19) that the contribution to $N_{QP}$ from the smaller electron surfaces is 0.26 that from the larger surfaces. The effective-mass measurements in figure 5 may now be expressed as $N_{QP}$ for comparison with the thermodynamic value $N_{SH}$ obtained from the specific-heat measurements of Muller *et al* [12] using equation (2), the result being shown as squares in figure 7. The full curve, as in figure 5, is the best fit to the theory of Wasserman *et al* [26].

**Table 3.** Summary of the parameters used to calculate the contribution to the quasiparticle density of states $\Delta N_{QP}$ in $CeB_6$, arising from the 'neck' regions of the Fermi surface. The parameters are defined in the appendix and with reference to figure A1. $F_n$ is obtained from the angle-resolved DHVA-effect measurements of Onuki *et al* [13], $m_n$ is the estimated effective mass of the neck orbit, which is found to be insensitive to the other parameters, and $A''$ is the curvature factor in equation (5).

| $F_n$ | $k_n$ | $k_x(\max)$ | $k_z(\theta_{max})$ | $\Delta k$ | $\theta_{max}$ | $r'$ | $m_n$ | $A''$ |
|---|---|---|---|---|---|---|---|---|
| 910 | $1.7 \times 10^9$ | $3.0 \times 10^9$ | $1.5 \times 10^9$ | 1.25 | 1.2 | 0.63 | 15 | $\sim 16$ |

Finally, to these values of $N_{QP}$ must be added the contribution from the 'neck' regions of the Fermi surface. The low quasiparticle velocity in these regions will lead, from equation (1), to a significant contribution to the density of states. Although this contribution will depend on the details of the Fermi surface topology and dynamical properties of quasiparticles in the neck region, it may be estimated, as shown in the appendix below, by using a simple hyperbolic approximation that each neck region contributes an amount $\Delta N_{QP}$ to $N_{QP}$,

$$\Delta N_{QP}(E_F) = (m_e/\pi^2\hbar^2)(2e/\hbar)^{1/2} F_n^{1/2}(m_n^* r'/m_e) \sinh\theta_{max} - \varepsilon(\theta_{max}, r') \quad (20)$$

where $F_n$ and $m_n^*$ are the neck frequency and mass respectively and $r'$ and $\theta_{max}$ are parameters defined with reference to figure A1. The quantity $\varepsilon(\theta_{max}, r')$ accounts for the portion of the ellipsoidal surface 'replaced' by the neck region, and we have used the value $F_n = 910 \pm 100$ T, inferred from the angle-resolved DHVA-effect measurements of Onuki *et al* [13]. Calculation yields a value for $m_n^* \simeq 15m_e$, which is rather insensitive to the fitting parameters, and shows that $\Delta N_{QP}$ is linearly related to the ellipsoid separation parameter $\Delta k$,

$$\Delta N_{QP}/N_{QP} = 3.6 \times 10^{-10} \Delta k.$$

These model calculations show that by choosing $\Delta k = 1.25 \times 10^9$ m$^{-1}$, a value that is reasonable and unexceptional, $N_{QP}$ and $N_{SH}$ are brought into excellent agreement, as illustrated by the broken curve in figure 7. The parameters used for these calculations are summarized in table 3. We note finally that applying the same analysis to $LaB_6$, we obtain a value for $N_{QP}$ within 2% of $N_{SH}$ derived from its electronic specific-heat coefficient of $\gamma = 2.6$ mJ mol$^{-1}$ K$^{-2}$.

We conclude therefore that the low-temperature thermodynamics of $CeB_6$ may be understood simply in terms of the low-energy excitations of a heavy charged Fermi liquid. In the antiferroquadrupolar phase, in which all of these experiments were conducted, $CeB_6$ is an example of a heavy-fermion system in which the volume of the Fermi surface has been

little changed by interaction with 4f electrons. In this respect it differs from $UPt_3$, in which the 5f electrons are, through hybridization, clearly itinerant [2]. Finally, we note that our experiments do not appear to support the idea of Kagan *et al* that a significant contribution to the low-temperature thermodynamics of Ce-based heavy-fermion systems arises from the presence in them of a neutral Fermi liquid.

**Acknowledgments**

We warmly acknowledge many helpful discussions with H Harima, S Hayden, Y Kagan and A Wasserman. The financial support of the Science and Engineering Research Council is also gratefully acknowledged.

## Appendix. Modelling the ellipsoidal and hyperboloidal regions of the Fermi surface of $CeB_6$ to obtain the density of states

To describe a prolate ellipsoidal Fermi surface (with its major axis directed along the $k_z$ axis), we may use a parabolic approximation for the dispersion relation

$$E_F = \hbar^2 k_x^2/2m + \hbar^2 k_y^2/2m + \hbar^2 k_z^2/2r^2 m. \tag{A1}$$

Considering only the $k_x$, $k_z$ plane for simplicity, the Fermi surface can be represented by the parametric equations for an ellipse

$$k_x = k_0 \cos\phi \qquad k_z = rk_0 \sin\phi' \tag{A2}$$

$k_0$ and $rk_0$ are the minor and major axes respectively and $\phi$ is the angle subtended by the vector $\boldsymbol{k}(\phi) = (k_x, k_z)$ from the $k_x$ axis.

To calculate the density of states using equation (1), we use polar coordinates and approximate the surface element $\partial S$ in figure A1($a$) by

$$\partial S = 2\pi k_x \partial l \equiv 2\pi k_0 \cos\phi \partial l \tag{A3}$$

where

$$\partial l = -k_0 \sqrt{\sin^2\phi + r^2\cos^2\phi}\,\partial\phi \tag{A4}$$

is the length of the arc subtended on the perimeter of the ellipse by the angular increment $\partial\phi$. Similarly, the Fermi velocity is given by

$$|v^*| = |(1/\hbar)\nabla_k E| = (\hbar k_0/rm)\sqrt{r^2\cos^2\phi + \sin^2\phi} \tag{A5}$$

which yields for the density of states

$$N_{QP}(E_F) = \frac{k_0 rm}{2\pi^2\hbar^2} \int_{-\pi/2}^{\pi/2} -\cos\phi\,\partial\phi. \tag{A6}$$

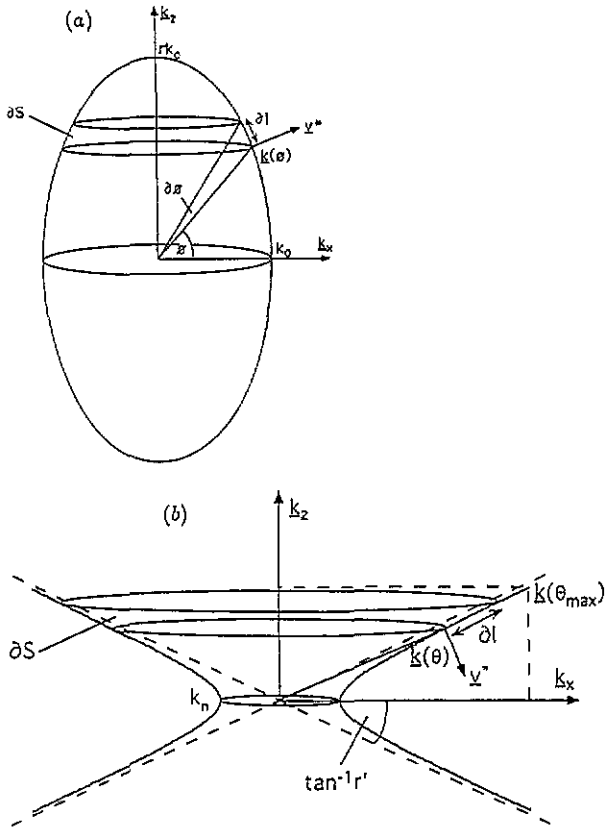


**Figure A1.** Geometry of (*a*) the ellipsoidal and (*b*) the hyperboloidal sheets of the Fermi surface used to calculate their contributions to the density of states in $CeB_6$.

Hence, writing for the minimum cross section of the ellipse $(\hbar/2e)k_0^2 = F_{min}$, with effective mass $m^*_{min}$, we obtain upon substitution equation (19) in the text

$$N_{QP}(E_F) = (m_e/\pi^2\hbar^2)(2e/\hbar)^{1/2}F_{min}^{1/2}(m^*_{min}/m_e)r. \tag{A7}$$

In section 6 we noted that, for the larger ellipsoidal Fermi surface in $CeB_6$, the relation $m^* \propto F$ has been found experimentally. For an arbitrary classical orbit, the cyclotron mass is given by

$$m^* = \frac{eB}{2\pi}\oint \partial t \tag{A8}$$

where

$$\partial t = (\hbar/eB)\partial l/|v^*(\phi)| \tag{A9}$$

$\partial t$ being the element of time that the quasiparticle spends on each part of its trajectory. Combining equations (A4), (A5) and (A8), we obtain $m^* = rm$ and, since the Fermi surface maximum cross-sectional area is also proportional to $r$, we obtain the relation

$m^* \propto F$. More generally, it can be shown that the mass $m(k)$ at any point on the Fermi surface is given by the relation

$$m(k) = \hbar^2(\partial^2 E/\partial|k|^2)^{-1} = m|k|^2/k_0^2. \tag{A10}$$

We model the neck regions in $CeB_6$ by hyperbolae of revolution, as shown in figure A1(*b*), in which case the dispersion relation may be written

$$E_F = \hbar^2 k_x^2/2m_n + \hbar^2 k_y^2/2m_n + E' - \hbar^2 k_z^2/2r'^2 m_n \tag{A11}$$

where $E'$ is an energy shift required to maintain the same chemical potential. As for the ellipse, the hyperbola can also be represented parametrically,

$$k_x = k_n \cosh\theta \qquad k_z = r' k_n \sinh\theta. \tag{A12}$$

The value $r'$ is now the tangent of the angle between the asymptote and the $k_x$ axis, $k_n$ is the radius of the neck, and $\theta$ a parameter from which $k(\theta)$ can be determined. Following the same procedure as for the ellipse, one finds that the density of states is modified by a factor $\sinh\theta_{max}$,

$$\Delta N_{QP}(E_F) = (m_e/\pi^2\hbar^2)(2e/\hbar)^{1/2} F_n^{1/2}(m_n^*/m_e) r' \sinh\theta_{max} \tag{A13}$$

which is equation (20) in the text, in which $F_n$ and $m_n$ refer to the neck frequency and mass respectively. Whereas in the ellipsoidal model the integration (26) was performed for $-\frac{1}{2}\pi < \phi < \frac{1}{2}\pi$, in the hyperboloidal case the integration is performed over the interval $-\theta_{max} < \theta < \theta_{max}$ where $\theta_{max}$ corresponds to the point in $k$ space ($k(\theta_{max})$) where the hyperbolic neck is tangent to the ellipsoid and the two surfaces have equal Fermi velocities.

## References


[1] Springford M 1991 *Physica* B **171** 151
[2] Taillefer L, Flouquet J and Lonzarich G G 1991 *Physica* B **169** 257
[3] Onuki Y, Goto T and Kasuya T 1991 *Materials Science and Technology* vol 3A (Weinheim: VCH) ch 7
[4] Effantin J M, Rossat-Mignod J, Burlet P, Bartholin H, Kunii S and Kasuya T 1985 *J. Magn. Magn. Mater.* **47 & 48** 145
[5] Regnault L P, Erkelens W A C, Rossat-Mignod J, Vettier C, Kunii S and Kasuya T 1988 *J. Magn. Magn. Mater.* **76 & 77** 413
[6] Effantin J M, Burlet P, Rossat-Mignod J, Kunii S and Kasuya T 1982 *Proc. Int. Conf. on Valence Instabilities (Zurich)* ed P Wachter and H Boppart (Amsterdam: North-Holland) p 559
[7] Bredl C D 1987 *J. Magn. Magn. Mater.* **63 & 64** 372
[8] Etourneau J, Mercurio J P, Naslain R and Hagenmuller P 1970 *J. Solid State Chem.* **2** 332
[9] van Deursen A P J, Fisk Z and de Vroomen A R 1982 *J. Less-Common Met.* **44** 609
[10] van Deursen A P J, Pols R E, de Vroomen A R and Fisk Z 1985 *J. Less-Common Met.* **111** 331
[11] Joss W, van Ruiteenbeek J M, Crabtree G W, Tholence J L, van Deursen A P J and Fisk Z 1987 *Phys. Rev. Lett.* **59** 1609
[12] Muller T, Joss W, van Ruitenbeek J M, Welp U, Wyder P and Fisk Z 1988 *J. Magn. Magn. Mater.* **76 & 77** 35
[13] Onuki Y, Komatsubara T, Reinders P H P and Springford M 1989 *J. Phys. Soc. Japan* **58** 3698
[14] Onuki Y, Nishihara M, Sato M and Komatsubara T 1985 *J. Magn. Magn. Mater.* **52** 317
[15] Ishizawa Y, Tanaka T, Bannai E and Kawai S 1977 *J. Phys. Soc. Japan* **42** 112
[16] Ishizawa Y, Nozaki H, Tanaka T and Nakajima T 1980 *J. Phys. Soc. Japan* **48** 1439
[17] Hasegawa A and Yanase A 1977 *J. Phys. F: Met. Phys.* **2** 1245
[18] Harima H, Sakai O, Kasuya T and Yanase A 1988 *Solid State Commun.* **66** 603

[19] Langford H D, Temmerman W M and Gehring G A 1990 *J. Phys.: Condens. Matter* **2** 559
[20] Haanappel E G, Hedderich R, Joss W, Askenazy S and Fisk Z 1992 *Physica* B **177** 181
[21] Kagan Yu, Kikoin K A and Prokof'ev N V 1992 *Physica* B **182** 201
[22] Kagan Yu, Kikoin K A and Prokof'ev N V 1992 *JETP Lett.* **56** 219
[23] Kagan Yu, Kikoin K A and Prokof'ev N V 1993 *Physica* B at press
[24] Harrison N, Meeson P, Probst P-A and Springford M 1993 *Meas. Sci. Technol.* **4** 148
[25] Lifshitz I M and Kosevich A M 1955 *Zh. Eskp. Teor. Fiz.* **29** 730
[26] Wasserman A, Springford M and Hewson A C 1989 *J. Phys.: Condens. Matter* **1** 2669
[27] Rasul J W 1989 *Phys. Rev.* B **39** 663
[28] Shoenberg D 1984 *Magnetic Oscillations in Metals* (Cambridge: Cambridge University Press) ch 9
[29] Sato N, Satoru S, Oguro I, Komatsubara T and Kasuya T 1984 *J. Phys. Soc. Japan* **53** 3967
[30] Joss W, van Ruitenbeek J M, Crabtree G W, Tholence J L, van Deursen A P J and Fisk Z 1989 *J. de Physique* **49** NC-8 747
[31] Matsui H, Goto T, Kunii S and Sakatsume S 1993 *Physica* B **188** 126
[32] Horn S, Steglich F, Loewenhaupt M, Scheuer H, Felsch W and Winzer K 1981 *Z. Phys.* B **42** 125